Slow-Nonlinearity Assisted Supercontinuum Generation in a CS_2-Core Photonic Crystal Fiber

Zhe Kang, Feng Xu, Jinhui Yuan, *Senior Member, IEEE, Senior Member, OSA*, Feng Li, *Senior Member, OSA*, Binbin Yan, Xian Zhou, *Member, IEEE*, Qiang Wu, Kuiru Wang, Xinzhu Sang, Keping Long, *Senior Member, IEEE*, and Chongxiu Yu

***Abstract*—In this paper, we theoretically investigate the supercontinuum generations (SCGs) in a carbon disulfide (CS_2)-core photonic crystal fiber (PCF). We show that the intrinsic slow-nonlinearity of CS_2 plays a significant role to control the soliton fission process. The initiation of the soliton fission process can be distinctly delayed. More importantly, the transition between the smooth soliton fission and the sub-solitons' chaotic-like interference is sufficiently extended so that the optical spectrum can keep broadening continuously while still maintain a smooth spectral profile. When pumping a designed CS_2-core PCF at wavelength 1.55 μm in the anomalous dispersion region, we obtain temperature-controllable and highly coherent SCs spanning over one-octave at the -30 dB spectral intensity. The unique feature of large slow-nonlinearity and the controllable dispersion and nonlinearity of CS_2-core PCF confirm it as a versatile platform for highly coherent and octave-spanning SCGs.**

***Index Terms*—CS_2-core photonic crystal fiber, slow-nonlinearity, supercontinuum generation**

I. Introduction

Supercontinuum generation (SCG) occurs when the incident optical pump field experiences strong nonlinear spectral broadening [1]. Since the first time supercontinuum (SC) was observed in bulk glass, it has been attracting extensive attentions in applications such as optical communications [2,3], spectroscopy [4,5], optical microscopy [6], optical coherence tomography [7], and optical frequency synthesis [8], etc. Photonic crystal fiber (PCF) has been confirmed to be an excellent nonlinearity media for SCGs due to its distinct optical characteristics, e.g. endless single-mode propagation, enhanced modal confinement, and flexibly adjustable dispersion and nonlinearity [1,9]. Coherence and bandwidth are the two significant performance targets to evaluate the quality of the SCs generated [1,10-12]. It is known that when pumping in the normal dispersion region, the coherence of the SCs generated can be very high [13]. This is because soliton dynamics which will cause the chaos in the spectra can be depressed in normal dispersion region. However, the superior coherence is obtained at the expense of narrow spectral bandwidth since the dominating nonlinear effect for the SCG is self-phase modulation (SPM) only. In contrast, when pumping in the anomalous dispersion regime, other Kerr and high-order nonlinearities contribute to rich nonlinear phenomena. Combined with the perturbation of high-order dispersion, featured dynamics like soliton fission, resonant dispersive-wave radiation, and soliton self-frequency shift frequently occur to extend the spectral extent significantly. But, the modulation instability (MI) effect in this regime does harm to the coherence of the generated SCs. When the pump pulses are short enough (< 100 fs), the influence of the MI will be greatly reduced ,which promises high coherence between spectrum shots [1,14,15]. Despite this, the superior coherence is typically maintained when the propagation length just passes the soliton fission point. If the solitons have split completely, sub-solitons' interference will occur and result in chaotic-like temporal profiles, which creates a marginal increase in the spectral broadening at the expense of the coherence [1,16]. Such coherence degradation becomes more serious for the cases of ultra-large order soliton numbers. It therefore imposes a restriction that the SCG has to be stopped at the propagation length only a few longer than the soliton fission point, which however does not reach the limit of spectral broadening. Such contradiction commonly exits in the SCGs using conventional silica, chalcogenide, or Group IV nonlinear materials.

Recently, the fibers with the core region filled with liquids, e.g. carbon disulfide (CS_2), carbon tetrachloride (CCl_4), toluene, and nitrobenzene etc., have attracted great interests

Manuscript received at 13 January, 2019.

This work is partly supported by the National Natural Science Foundation of China (61875238 and 61475023), Beijing Youth Top-notch Talent Support Program (2015000026833ZK08), Fund of State Key Laboratory of Information Photonics and Optical Communications (Beijing University of Posts and Telecommunications) P. R. China (IPOC2017ZZ05), Shenzhen Science and Technology Innovation Commission (JCYJ20160331141313917), and Research Grant Council of Hong Kong (PolyU152144/15E).

Zhe Kang and Feng Xu contributed equally to this paper. The corresponding authors: Jinhui Yuan and Feng Li, e-mails: yuanjinhui81@bupt.edu.cn, enlf@polyu.edu.hk.

Zhe Kang, Feng Xu, Jinhui Yuan, Binbin Yan, Kuiru Wang, Xinzhu Sang, and Chongxiu Yu are with the State Key Laboratory of Information Photonics and Optical Communications, Beijing University of Posts and Telecommunications (BUPT), Beijing 100876, China.

Zhe Kang, Jinhui Yuan and Feng Li, are with the Photonics Research Centre, Department of Electronic and Information Engineering, The Hong Kong Polytechnic University, Hung Hom, Hong Kong, China.

Feng Li is also with the Hong Kong Polytechnic University Shenzhen Research Institute, 518057, Shenzhen, China.

Xian Zhou and Keping Long are with the school of Computer and Communication Engineering, University of Science and Technology Beijing (USTB), Beijing 100083, China.

Qiang Wu is with the Department of Physics and Electrical Engineering, Northumbria University, Newcastle upon Tyne, NE1 8ST, United Kingdom.

due to their large nonlinear refractive indices n_2 (~2-orders of magnitude larger than pure silica, close to silicon) and good transparency from the visible to the infrared spectral region [17-22]. Among these nonlinear liquids, CS_2 shows prominent characteristics that are conducive to nonlinear applications. Due to its linear molecular composition, the transparency of CS_2 thin cells broadly covers from the visible region to deep mid-infrared region of up to 12 μm except for the narrow isolated spectral region around 4.6 and 6.6 μm [23]. Moreover, a distinct nonlinearity, namely slow-nonlinearity (also named as non-instantaneous, reorientational, or retarded nonlinearity), has been revealed by CS_2 liquid [17,18,22,24,25]. Such slow-nonlinearity plays a significant role in SCGs besides the Kerr-nonlinearity because its contribution shows large proportion of nearly 85.7% of the whole nonlinearity. The influences of slow-nonlinearity on the broadening of SCs have been focused in the schemes reported so far. Only brief descriptions have been given to declare that the slow-nonlinearity can also enhance the coherence of SCs [17,18], but still rare details have ever been shown [22]. Moreover, it remains unclear how the dynamic of SCGs perturbed by this slow-nonlinearity connects to those of the instantaneous Kerr mediums.

In this paper, we investigate in detail the role of slow-nonlinearity of a CS_2-core PCF in enhancing the coherence of SCs for the first time. The slow-nonlinearity will effectively retard soliton fission caused by Kerr-nonlinearity. In addition, the slow-nonlinearity can also keep broadening the SCs in a long propagation length after the soliton fission point while sustaining its high coherence. We also investigate the performance of SCGs affected by the hybrid nonlinearity of the CS_2-core PCF under different influence factors, e.g. pump parameters and temperature. Octave-spanning and highly coherent SCs are finally demonstrated when all the factors are considered.

II. Theoretical Models

A. Propagation equation

The optical field propagating inside the CS_2-core PCF is governed by the modified generalized nonlinear Schrödinger equation (GNLSE) with slow-nonlinearity included,

$$\frac{\partial U}{\partial z}+\sum_{2}^{n}\beta_k\frac{i^{k-1}}{k!}\frac{\partial^k U}{\partial t^k}=i\gamma\left(1+i\frac{\gamma_1}{\gamma}\frac{\partial}{\partial t}\right)\Big[(1-f_{\mathrm{m}})\,|U(z,t)|^2 U(z,t)+f_{\mathrm{m}}\,\mu U(z,t)\int_0^{+\infty}e^{-\mu\tau}\left|U(t-\tau)\right|^2\mathrm{d}\tau\Big], \tag{1}$$

where $U(z, t)$ is the slowly varying envelop of the electrical field, z and t are the propagation distance and retarded time scale, respectively. β_k is the k-th order dispersion coefficient. The dispersion term is calculated in the Fourier domain by $\{\beta(\omega) - \beta(\omega_0) - \beta_1(\omega_0)(\omega - \omega_0)\}\hat{U}(\omega)$ to accurately present the dispersion characteristics within a broad wavelength region. $\gamma(\omega_0)$ is the nonlinear coefficient calculated by,

$$\gamma=\frac{\omega_0}{c}\frac{\iint n_2(x,y)\left|E(x,y)\right|^4 dxdy}{\left(\iint\left|E(x,y)\right|^2 dxdy\right)^2}, \tag{2}$$

where c is the velocity of the light in vacuum, ω_0 is the central angular frequency, $n_2(x, y)$ is the nonlinear refraction index. As the spectrum of the generated SCs covering a broadband spectral region, the wavelength dependence of γ are taken into account by using $\gamma_1 = \mathrm{d}\gamma/\mathrm{d}\omega$, as given by [1],

$$\frac{\gamma_1}{\gamma}=\frac{1}{\omega_0}+\frac{1}{n_2}\left(\frac{\mathrm{d}n_2}{\mathrm{d}\omega}\right)_{\omega=\omega_0}-\frac{1}{A_{\mathrm{eff}}}\left(\frac{\mathrm{d}A_{\mathrm{eff}}}{\mathrm{d}\omega}\right)_{\omega=\omega_0}, \tag{3}$$

where A_{eff} is the effective mode area. Inside the square brackets on the right side of Eq. (1), the first component represents the Kerr effects contribution, and the second component represents slow-nonlinearity contribution. f_{m} is the slow-nonlinearity parameter to quantify the fraction of the slow-nonlinearity, which is 6/7 for CS_2 material [17,18]. The response function of the slow-nonlinearity is a temporal exponential decay function $\mu e^{-\mu t}$, where the decay rate μ = 10 ps^{-1} [18,26]. Because the fraction of the slow-nonlinearity in the whole nonlinearity reaches up to 6/7, the Raman nonlinearity can be neglected [17]. The two- and multi-photon absorption of CS_2 are also negligible within the wavelength region considered [18,22]. Due to the intrinsic low material loss of CS_2, the predictable low confinement loss as a result of the tight mode confinement of the proposed PCF, and the short fiber length utilized, the linear propagation loss is safely neglected in our simulation [17,18,23]. The fourth-order Runge-Kutta algorithm is used to numerically solve Eq. (1).

B. Degree of first-order coherence

The degree of first-order coherence is used to quantify the coherence of the generated SCs, as given by [1,10,12],

$$\left|g_{1,2}^{(1)}(\lambda,t_1-t_2)\right|=\left|\frac{\left\langle U_1^*(\lambda,t_1)U_2(\lambda,t_2)\right\rangle}{\left\langle\left|U_1(\lambda,t_1)\right|^2\right\rangle\left\langle\left|U_2(\lambda,t_2)\right|^2\right\rangle}\right|, \tag{4}$$

$A(\lambda, t)$ is the spectral amplitude. The angular brackets represent the ensemble average over independent spectrum pairs, i.e. $\hat{U}_1(\lambda, t)$ and $\hat{U}_2(\lambda, t)$, which are obtained from 100 shot-to-shot simulations with the random noise perturbation. The random photon noise is defined as $\sigma=\eta\tilde{U}\exp(i2\pi\tilde{N})$, where η is the noise amplitude, $\tilde{U}$ is a normally distributed random variable, and $\tilde{N}$ is a uniformly distributed variable between 0 and 1. The coherence is calculated at $t_1 - t_2 = 0$.

To quantitatively analyzing the overall coherence spanning the SC spectrum, a spectrally averaged coherence is given by [1,10],

$$<\left|g_{1,2}^{(1)}\right|>=\frac{\int\left|g_{12}^{(1)}(\lambda,0)\right|\left|U(\lambda)\right|^2 d\lambda}{\int\left|U(\lambda)\right|^2 d\lambda}, \tag{5}$$

where $<\left|g_{1,2}^{(1)}\right|>$ is a positive value within [0, 1]. Furthermore, the coherence of SC is proportional to $<\left|g_{1,2}^{(1)}\right|>$.

III. Design of the CS_2-core PCF

The cross-section of the proposed CS_2-core PCF is shown in Fig. 1(a). The geometry of the PCF is a standard hexagon. The core of the PCF is filled with CS_2 and surrounded by three layers of air holes in the fused silica cladding. The radiuses of the core and the air hole are r_1 = 0.9 μm and r_2 = 0.8 μm, respectively. The distance between the air holes is Λ = 2.2 μm. The electrical field distribution is calculated by using the full vector finite element method. Figs. 1(b), 1(c), and 1(d) show the electrical field profiles of the fundamental mode at 1.3, 1.6, and 2.3 μm, respectively. We observe that the designed CS_2-core PCF can confine the optical modes tightly in the core region even at 2.3 μm. The refractive index of CS_2 at 20 °C is given by the Sellmeier equation [27],

$$n_{CS_2} = 1.580826 + 1.52389\times10^{-2}\lambda^{-2} + 4.8578\times10^{-4}\lambda^{-4} - 8.2863\times10^{-5}\lambda^{-6} + 1.4619\times10^{-5}\lambda^{-8}, \quad (6)$$

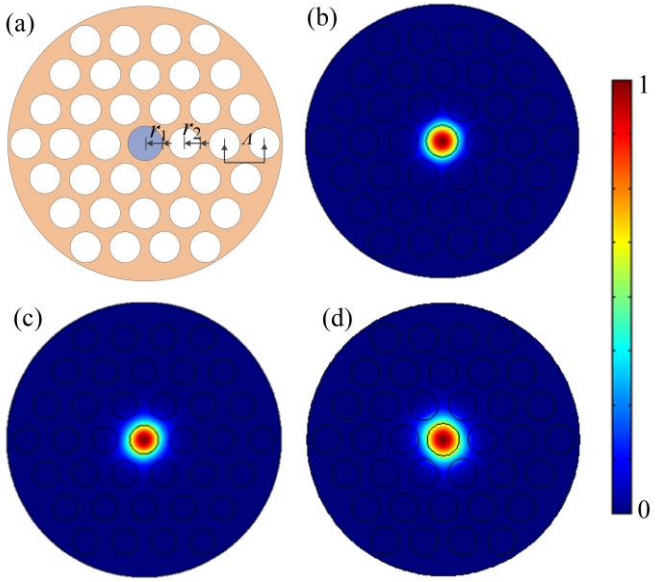

Fig. 1. (a) Cross-section of the proposed CS_2-core PCF. (b), (c), and (d) The electrical field profiles of the fundamental mode at wavelengths 1.3, 1.6, and 2.3 μm, respectively.

When pumping near the zero-dispersion wavelength in the anomalous dispersion regime, the phase-matching condition is easy to be met so that strong four-wave mixing (FWM) effect can be excited for broadband SCG. Operation near zero-dispersion wavelength also enhances the perturbation of high-order dispersion, thus radiating strong resonant dispersive waves that filling up the spectrum in the normal dispersion regime. We optimize the geometrical parameters Λ and r_2 to tailor the dispersion characteristics of the proposed CS_2-core PCF, while r_1 is fixed to a constant of 0.9 μm. The calculated dispersion parameters $D = -2\pi c\beta_2/\lambda^2$ as a function of wavelength at different Λ and r_2 are shown in Figs. 2(a) and 2(b), respectively, under the room temperature of 20 °C. We observe that when Λ is increased, the zero-dispersion wavelength (ZDW) monotonously shifts towards the longer wavelength side. In contrast, when r_2 is increased, the zero-dispersion wavelength monotonously shifts towards the shorter wavelength side. The optimized geometrical parameters are found to be r_1 = 0.9, r_2 = 0.8, and Λ = 2.2 μm. The calculated dispersion parameters and nonlinear coefficients as a function of wavelength under this parameter configuration are shown in Figs. 2(c) and 2(d), respectively. The zero-dispersion wavelength is located at 1.537 μm. The nonlinear coefficient at 1.55 μm is found to be up to 3.81 $W^{-1}m^{-1}$, which is about 3-orders of magnitude larger than that of the traditional fused silica PCF.

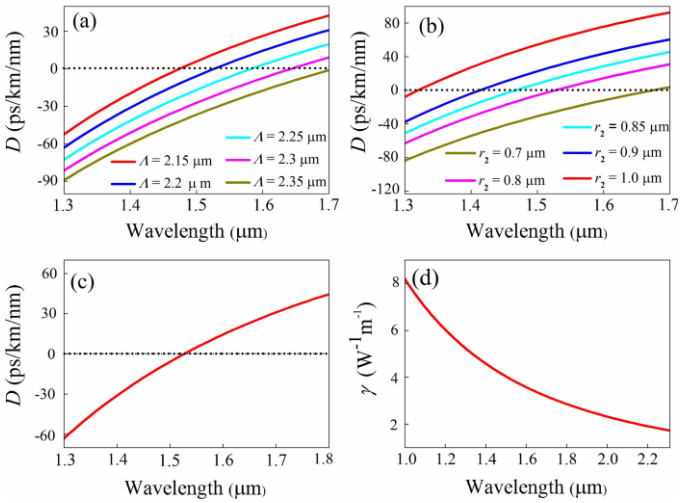

Fig. 2. Dispersion parameters as a function of wavelength under (a) different Λ and a fixed r_2 of 0.8 μm, (b) different r_2 and a fixed Λ of 2.2 μm. (c) Dispersion parameter and (d) nonlinear coefficient as a function of wavelength at Λ = 2.2 μm and r_2 = 0.8 μm. r_1 and temperature are kept the constants of 0.9 μm and 20 °C for all the cases.

IV. Results and Discussions

A. Influence of slow-nonlinearity

In order to reveal the contribution of slow-nonlinearity to the SCGs, we set the value of f_m to 0, 1, and 6/7 in the simulations, which correspond to the conditions with only Kerr-nonlinearity, only slow-nonlinearity, and both Kerr- and slow-nonlinearity, respectively. The pump source is assumed to be the hyperbolic secant shaped pulse at 1.55 μm. The pump pulse width T_0 and peak power P_0 are set as 80 fs and 1000 W, respectively, resulting in a high soliton number of N_{sol} = 85 given by the definition of $N_{sol} = (T_0^2\gamma P_0/|\beta_2|)^{1/2}$. Soliton fission in this case dominates the SCGs instead of MI effect. The propagation length L is set as 3 cm. Figs. 3(a)-3(c) show the temporal evolution profiles along with the temporal profiles at the input and output ends of the PCF when f_m is 0, 1, 6/7, respectively. Accordingly, the spectral evolution profiles and the spectral profiles are shown below in the Figs. 3(d)-3(f). The coherence is also estimated by doing 100 spectrum pairs statistical simulations with the noise amplitude of $\eta=1\times10^{-3}$.

Figures 3(a) and 3(d) show the dynamic of SCG follows a usual way when only Kerr-nonlinearity is considered (f_m = 0). In the time domain as shown in Fig. 3(a), the high-order soliton first experiences a compression process (stage I, 0 ~ 0.8 cm), then begins to smoothly eject sub-solitons as the soliton fission length is reached (stage II, 0.8 ~ 1.1 cm). A short propagation after the initiation of the soliton fission, the sub-solitons undergo nonlinear interactions and interference with each other due to the excessive nonlinearity and dispersion, which result in chaotic-like temporal profiles (stage III, 1.1 ~ 3 cm). Fig. 3(d) shows the spectral evolution is correspondingly divided into three distinct stages. The spectrum is first broadened moderately by the SPM dominated nonlinearity, along with the dispersion, compression process in the time domain is also shown in Fig. 3(d). When the soliton fission length is reached, the spectrum abruptly experiences an explosive broadening, but still maintaining smooth profiles. However, the stage II process only sustains 0.3 cm propagation length. The spectrum in the further stage III is more significantly broadened but becomes very complicated, which predictably corresponds to a low coherence. The upper inset of Fig. 3(a) shows the coherence at the output end remains a very low level within the whole wavelength region considered.

In comparison, we observe distinct delay of the soliton fission when the slow-nonlinearity exists. Fig. 3(b) shows the initiation of the soliton fission is delayed to 1.6 cm when only slow-nonlinearity exists (f_m = 1). Noticeably, only stage II process is observed in the following propagation till the 3 cm fiber length simulated. The sub-solitons are smoothly ejected without undergoing severe interference or other complex dynamics. This is because the slow-nonlinearity retards the soliton fission and the propagation length is not long enough for solitons to split completely. The post-ejected sub-soliton has enough time to wait the pre-ejected sub-soliton to be delayed away (spectrally red-shifted), thus avoiding the encounter and interference with each other. In contrast, the high-order soliton spits the sub-solitons very quickly when only Kerr-nonlinearity exists. The sub-solitons will largely aggregate and interfere with each other, thus quickly ends the stage II process. Moreover, we observe the compressed high-order soliton in the stage I process of Fig. 3(a) has strong and wide substrates, which undoubtedly will perturb the sub-solitons ejected in the stage II. Benefit from the retarded stage I process induced by the slow-nonlinearity, Fig. 3(b) shows the soliton is sufficiently compressed with weak and narrow substrates left which is benifical for high coherence. Fig. 3(e) shows the spectrum is continuously broadened in stage II with maintained smooth profiles. The spectra at the output end cover from 1.14 to 2.16 μm (~0.92-octave) at the -30 dB spectral intensity, and the coherence remains unity within this wavelength region.

Figs. 3(c) and 3(f) show that the joint interaction of Kerr- and slow-nonlinearity (f_m = 6/7), helps to enhance the spectrum broadening while still maintaining a superior coherence. The initiation of the soliton fission is 1.5 cm, which is 0.1 cm in advance than that of f_m = 1 due to the participation of Kerr-nonlinearity. Still no stage III process is observed. The spectrum in stage II is distinctly enhanced both in the red- and blue-side. Such enhancement already happens significantly when the soliton fission length is just past. The SC generated at the output end spans from 1.05 to 2.22 μm (~1.08-octave) at the -30 dB spectral intensity, which is much larger than the maximum bandwidths in stage II of both f_m = 1 (0.92-octave) and f_m = 0 (0.86-octave). The coherence remains unity except for the small dip around 1.07 μm.

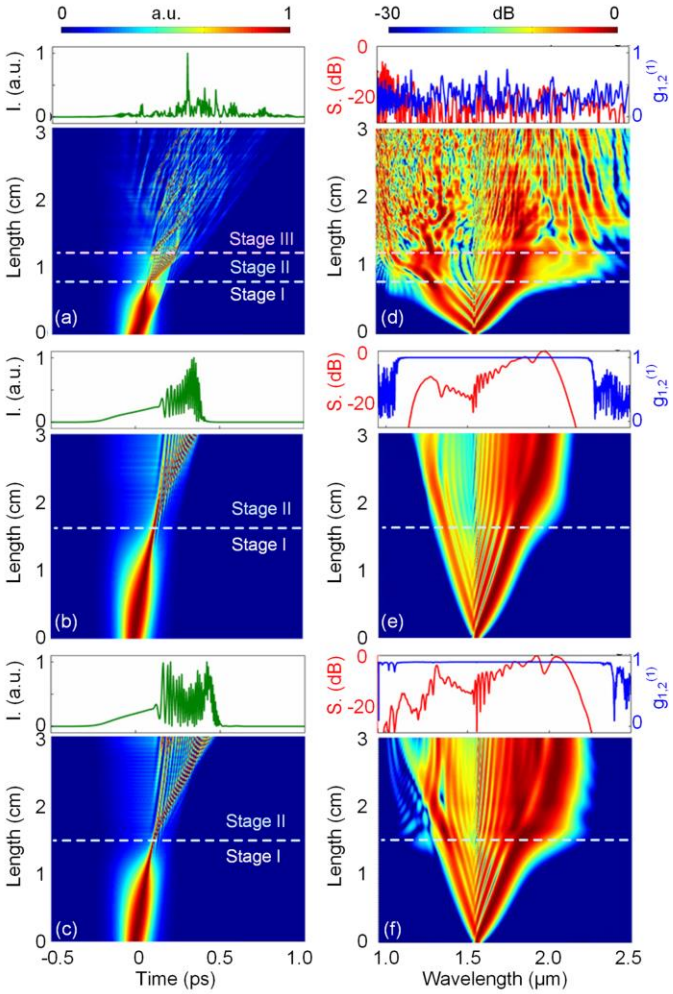

Fig. 3. Temporal and spectral evolution profiles, along with the temporal (green curves) and spectral (red curves) profiles at the output end of the PCF under (a) and (d) f_m = 0, (b) and (e) f_m = 1, (c) and (f) f_m = 6/7, respectively. The coherence is also estimated and shown in (d)-(f) (blue curves) by doing 100 pairs statistical simulations of the spectra with the noise amplitude of $\eta = 1 \times 10^{-3}$.

B. Influence of pump parameters

We study the influence of the pump pulse width on the performance of the SCG. The parameters used in the simulations are same to that in Figs. 3(c) and 3(f) except for a set of arbitrarily chosen pump pulse widths T_0 from 80 to 1600 fs. Fig. 4 shows the temporal and spectral profiles along with the coherence at the output end of the fiber. We see when T_0 is increased to several hundreds of femtoseconds, the MI effect instead of the soliton fission begins to dominant the SCG. The spectrum broadening is significantly limited even with the assistant of the slow-nonlinearity. The coherence also shows

bad performance. For example, the bandwidth of the SC generated is reduced to 0.58-octave at T_0 = 250 fs. The coherence shows severe degradation on the central region of the spectrum, resulting in an averaged coherence of only 0.71. When T_0 is increased to 1600 fs, the bandwidth of the SC and the averaged coherence are only 0.12-octave and 0.46, respectively. The results indicate that for narrow pulse, slow-nonlinearity can effectively maintain high coherence of the octave-spanning SC. However, with the increase of the pulse duration, the MI will have evident influence on the coherence, and the slow-nonlinearity cannot eliminate the effect of MI. Therefore, the coherence is degraded at this time.

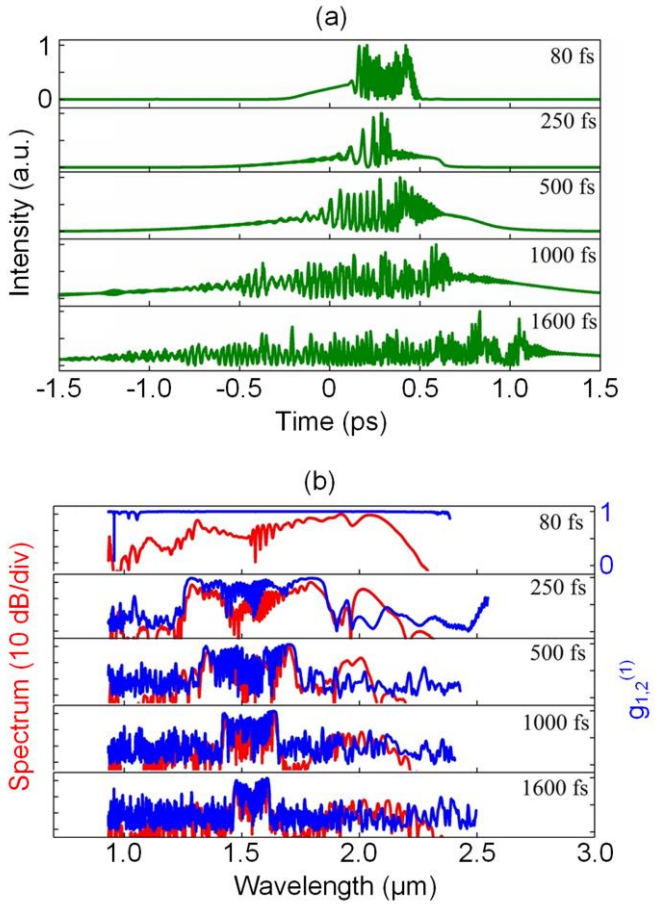

Fig. 4. (a) Temporal and (b) spectral profiles at the output end of the PCF when the pump pulse width is increased from 80 to 1600 fs. The coherence is also calculated and shown in blue curves.

We further study the influence of the pump peak power P_0 on the SCGs. The pump pulse width is fixed to 80 fs so that the soliton fission dominates the SCGs. The P_0 in the simulations are arbitrarily chosen from 100 to 3900 W, corresponding to the soliton number from 29 to 182, respectively. Although it's all increasing the soliton number, the SCGs show completely different results with respect to that in Fig. 4. Fig.5 shows that for the cases of $P_0 \leq$ 1300 W, the slow-nonlinearity can guarantee a superior coherence. However, when P_0 is increased to 2500 and 3900 W, the coherence is found to be significantly degraded, especially on the two border regions of the SC generated. With higher peak power, the blue-shifted dispersion waves will become more complicated and disordered. In addition, the coherence of SCs at short wavelength side is much degraded even with a small peak power of 500 W. Therefore, we deduce the coherence degradation is attributed to the perturbation of the enhanced dispersive waves. The temporal profiles of the enhanced dispersive waves overlap and interfere with the ejected sub-solitons, resulting in complicated modulation on both the temporal and spectral profiles, in turn causing the chaos of both temporal and spectral profiles. Less solitons will be split with the decrease of soliton numbers which is due to the deduction of the peak power, along with the accelerating soliton fission process in slow-nonlinearity, the generated SC is with a high coherence in lower peak power. In addition, more fluctuations of blue-shifted dispersion waves are shown in Fig. 5, so slow-nonlinearity cannot prevent the perturbation of strong dispersive waves. For a given pump pulse width and fiber configuration, there should be an upper limit of the pump peak power to maintain both broadband spectrum and superior coherence. Even so, it is predictable the bandwidths and coherence of the SCs generated in these cases could be better than those with only Kerr-nonlinearity, which already goes deep into the stage III dynamic shown in Fig. 3(a) when P_0 is 1000 W.

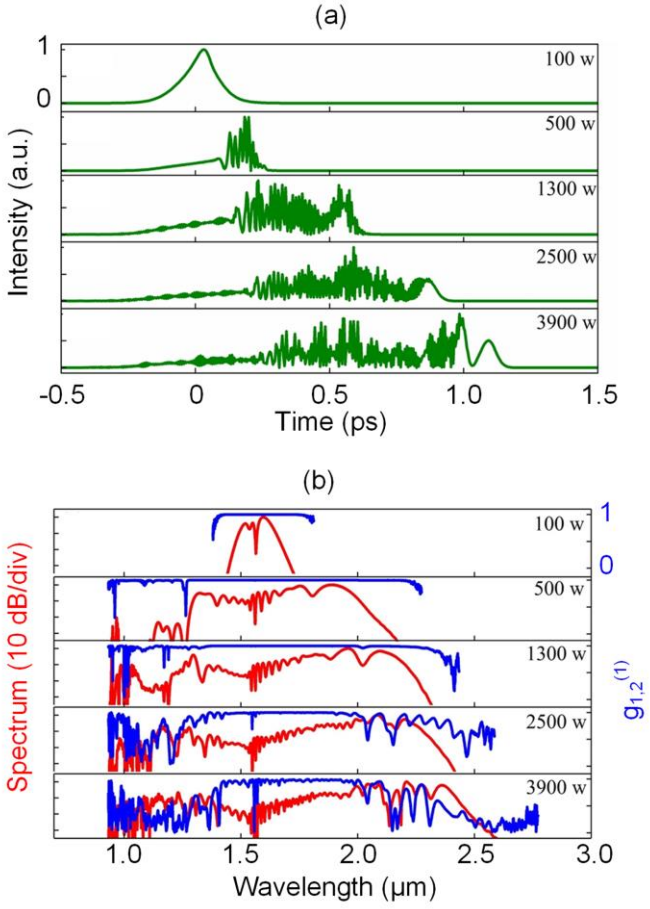

Fig. 5. (a) Temporal and (b) spectral profiles at the output end of the PCF when the pump peak power is increased from 100 to 3900 W. The coherence is shown in blue curves.

Fig. 6 shows the temporal and spectral profiles, along with

the coherence, at different propagation lengths. We see the SCG almost reaches the limit of broadening when the propagation length is 3.3 cm. Further increase of the length only results in the slight change of the spectral envelope. The coherence can be maintained very well when the propagation length is not more than 4.8 cm. For example, the coherence at length of 4.8 cm keeps unity within the wavelength region considered except for the two distinct dips around 1.14 and 1.96 μm. In contrast, when the length is increased to 6 cm, many dips of the coherence can be clearly seen. The coherence can only keep unity from 1.31 to 1.88 μm. The results indicate that the propagation length should not be very long even with the slow-nonlinearity, otherwise, the coherence would still be degraded because the interference of the solitons will be enhanced if the solitons have split completely.

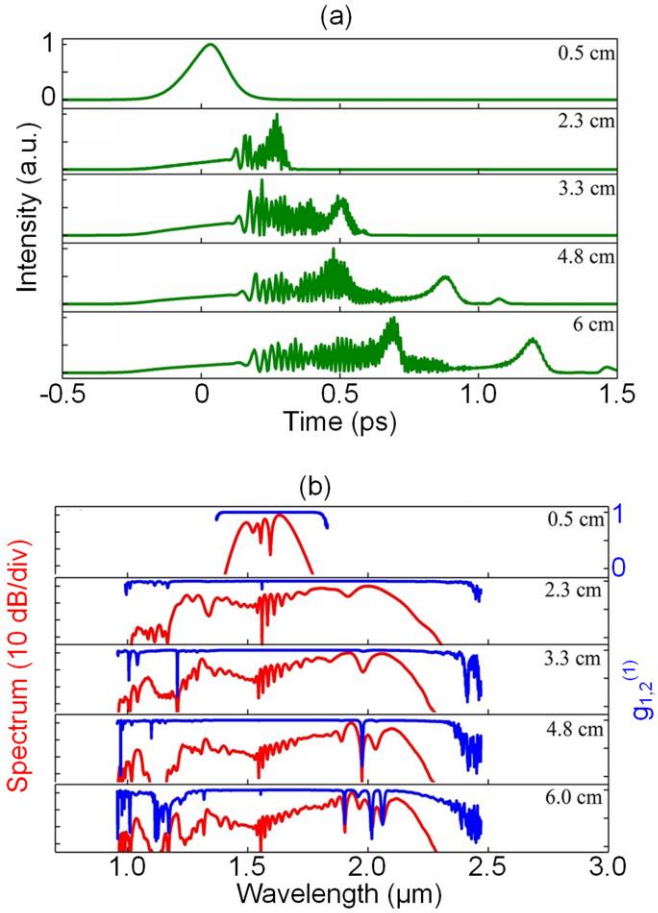

Fig. 6. (a) Temporal and (b) spectral profiles at the output end of the PCF when the propagation length is increased from 0.5 to 6.0 cm.

C. *Influence of temperature*

The refractive indices of CS_2 are sensitive to the temperature as following

$$n(\lambda,T) = n(\lambda) + \Delta T \frac{\mathrm{d}n}{\mathrm{d}T}, \tag{7}$$

where $n(\lambda)$ is the refractive index of CS_2 at the reference temperature of 20 °C at the wavelength λ, ΔT is the difference between the practical temperature T and the reference temperature 20 °C, $\mathrm{d}n/\mathrm{d}T$ is the variation rate of the refractive index with respect to T, which is -7.91×10^{-4} K^{-1} for CS_2 [28]. The refractive indices of silica affected by temperature are calculated by referring to the literature [29]. Fig. 7(a) shows the calculated second-order dispersion coefficient β_2 and the corresponding dispersion parameter D as a function of the temperature at λ = 1.55 μm. We can see the condition of anomalous dispersion is maintained, and the variation of β_2 with respect to temperature shows a parabolic shape. A maximum β_2 of -3.33 ps^2/km is obtained at T = 20 °C, corresponding to a maximum red-shifted zero-dispersion point within the temperature considered. The temperature induced refractive index variation also changes the effective mode area of the CS_2-core PCF and in turn the nonlinear coefficient. Fig. 7(b) shows the calculated γ and γ_1 as a function of the temperature. We see both of them monotonously decrease when the temperature is increased. Although the β_2 at T = 20 °C reaches a maximum (closest to the zero-dispersion point), the corresponding nonlinearities do not reach the maximums, meaning the SCG at T = 20 °C might not be optimal.

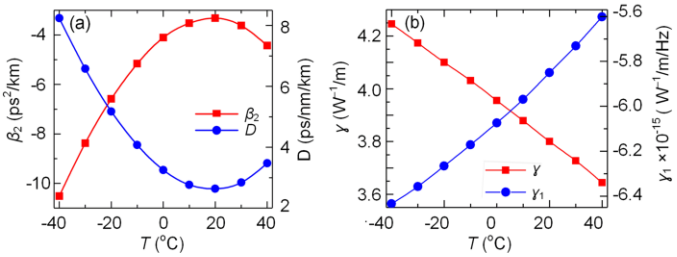

Fig. 7. The calculated (a) β_2 and D, (b) γ and γ_1 when temperature T varies from –40 to 40 °C.

We simulate the SCGs at T = -40, 0, and 40 °C, respectively, with the other parameters the same as that in Figs. 3(c) and 3(f). Fig. 8(a) shows the SC generated at T = 0 °C has broader -30 dB bandwidth of 1260 nm (1.02 ~ 2.28 μm, 1.16-octave), while the one at T = -40 °C has narrower bandwidth of 1175 nm (1.105 ~ 2.28 μm, 1.04-octave). The spectral intensity at T = 0 °C is also better than that obtained at the other two temperatures, meaning the optimized operation temperature is around 0 °C for the given CS_2-core PCF. Quantitatively, we calculated the -30 dB bandwidth and the averaged coherence from -40 to 40 °C with an interval of 10 °C. The SC generation is such a complicated process which is affected by the dispersion and nonlinearity, as shown in Fig 7. We cannot find some specific numerical relationships between the dispersion, nonlinearity and temperature. Figs. 8(b) and 8(c) show the relationships between the bandwidth, coherence and temperature. From Figs. 8(b) and 8(c), although there are some fluctuations between bandwidth and temperature, the bandwidth and coherence are fully temperature-controllable. Importantly, we find the bandwidths of all the SCs generated within the given temperatures exceed one-octave spanning. The corresponding averaged coherence also shows superior performance, i.e. all the degrees of the averaged coherence are larger than 0.9 except for the one of 0.894 at T = -20 °C. The characteristic of temperature-sensitive provides another degree of freedom besides the structures of

the CS_2-core PCF to control the SCGs, meanwhile without limiting the effectiveness of the slow-nonlinearity.

To interpret the time-frequency insights, we plot the spectrogram of the optimized SCG (T = 0 °C), as shown in Fig. 9(a). We see that the dynamic of soliton fission and dispersive wave generation can be clearly identified and correlated. In addition to buffer the soliton fission process, the slow-nonlinearity also shows a similar effect with Raman scattering, which induces the red-shift of soliton spectrum for the considered parameters, as shown in Fig. 9(a) and Fig. 3(f). The red-shifted spectral components of the sub-solitons are the main contributors to the SC of the longer wavelength side. Correspondingly, the dispersive waves generated and the FWM products between the dispersive waves and the solitons are the main contributors to the SC of the shorter wavelength side. The temporal profiles of the dispersive waves overlap and interfere with that of the sub-solitons, which confirms the discussion of Fig. 5. The oscillation structure around the central part of the spectrum is contributed by the SPM effect. The temporal profiles of this structure are weak and exist on the leading edge of the whole temporal profiles, which do not overlap with the temporal components of the sub-solitons and dispersive waves.

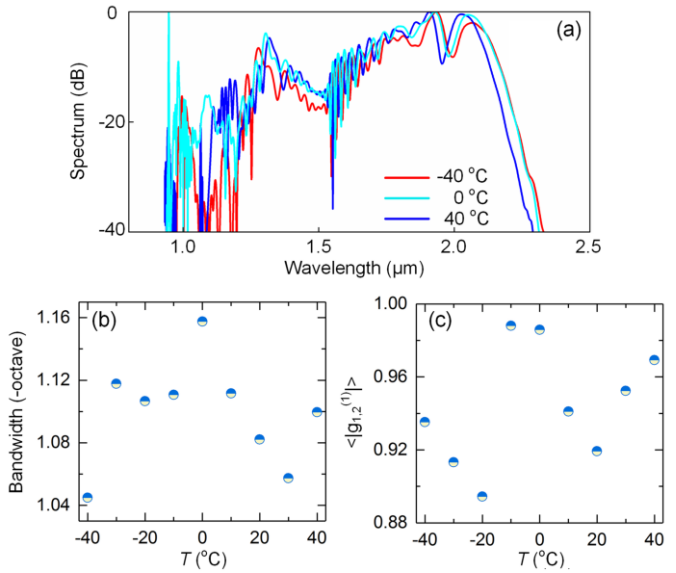

Fig. 8. (a) The SCs generated at –40, 0, and 40 °C, respectively. (b) The bandwidth and (c) the averaged coherence as the function of temperature.

We also estimate the coherence of the optimized SCG (T = 0 °C) at two different noise amplitudes. Figs. 9(b) and 9(d) show the stacked spectra (grey curves) and their average (blue curves) of the 100 statistical simulations at the noise amplitudes of $\eta = 10^{-3}$ and 10^{-2}, respectively. Figs. 9(c) and 9(e) show the corresponding coherence estimated. When the noise amplitude is $\eta = 10^{-3}$, we observe the spectra vary slightly from shot to shot except for the spectral component around 1.02 μm. The coherence estimated matches the variation of the spectra, which is kept unit from 1.02 to 2.28 μm except for the big dip around 1.02 μm. The averaged coherence of the spectra is calculated to be up to 0.984. In comparison, when the noise amplitude is increased to $\eta = 10^{-2}$, the spectra of each shot show larger variations and the coherence degrades obviously. Although, the coherence can only keep unit within the wavelengths spanning from 1.6 to 1.8 μm, the averaged coherence can still reach 0.842. Such performance confirms the good capability of noise-tolerance of the SCGs in CS_2-core PCF.

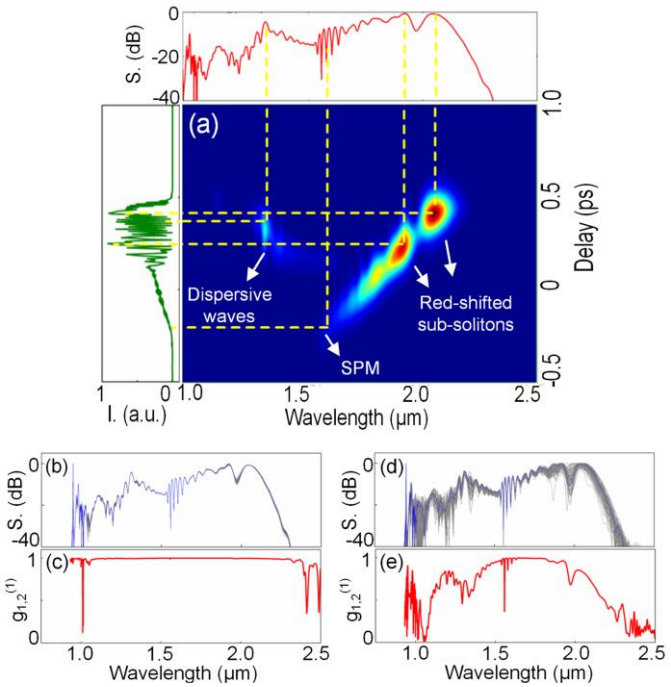

Fig. 9. Spectrogram of the optimized SCG (T = 0 °C). Left inset: temporal profile. Upper inset: spectral profile. The stacked spectra (grey curves), the averaged spectra (blue curves), and the coherence (red curves) of the 100 shots statistical simulations at (b) and (c) $\eta = 10^{-3}$, (d) and (e) $\eta = 10^{-2}$.

V. Conclusion

In summary, we investigate in detail the influences of slow-nonlinearity on the SCGs in the CS_2-core PCF. The slow-nonlinearity in CS_2-core PCF can retard the ejection of sub-solitons, thus smooth spectra can be maintained even in the process of–soliton fission. As a result, the SCs generated can easily be broadened over one octave-spanning, while still maintain the highly superior coherence. The structure of the designed CS_2-core PCF is simple and easy to be practically fabricated [30]. Moreover, thanks to the temperature-sensitivity of the refractive index and the photonic crystal structure, the CS_2-core PCF shows excellent capability of dispersion and nonlinearity tailoring. Along with the intrinsic highly nonlinear refractive index of CS_2, controllable SCs with octave-spanning bandwidth and high coherence are guaranteed to be achieved at the low expenses of pump energy and fiber length. Our study confirms the CS_2-core PCF as a versatile platform for highly coherent and octave-spanning SCGs from near- to mid-infrared spectral region, which paves the way for many applications in spectroscopy, metrology, optical sensing, etc.

References

[1] J. M. Dudley, G. Genty, and S. Coen, “Supercontinuum generation in photonic crystal fiber,” *Rev. Mod. Phys.* vol. 78, no. 4, pp. 1135–1184, Oct. 2006.

[2] T. Morioka, S. Kawanishi, K. Mori, and M. Saruwatari, "Transform-limited, femtosecond WDM pulse generation by spectral filtering of gugahertz supercontinuum," *Electron. Lett.* vol. 30, no. 14, pp. 1166–1168, Jul. 1994.

[3] K. R. Tamura, H. Kubota, and M. Nakazawa, "Fundamentals of stable continuum generation at high repetition rates," *J. Quantum Electron.* vol. 36, no. 7, pp. 773–779, Jul. 2000.

[4] J. Hult, R. S. Watt, and C. F. Kaminski, "High bandwidth absorption spectroscopy with a dispersed supercontinuum source," *Opt. Express*, vol. 15, no. 8, pp. 11385–11395, Sep. 2007.

[5] K. B. Shi, P. Li, and Z. W. Liu, "Broadband coherent anti-Stokes Raman scattering spectroscopy in supercontinuum optical trap," *Appl. Phy. Lett.* vol. 90, no. 14, pp. 141116, Apr. 2007.

[6] C. F. Kaminski, R. S. Watt, A. D. Elder, J. H. Frank, and J. Hult, "Supercontinuum radiation for applications in chemical sensing and microscopy," *Appl. Phys. B.* vol. 92, no. 3, pp. 367–378, Sep. 2008.

[7] I. Hartl, X. D. Li, C. Chudoba, R. K. Ghanta, T. H. Jo, J. G. Fujimoto, K. K. Ranka, and R. S. Windeler, "Ultrahigh resolution optical coherence tomography using continuum generation in an air-silica microstructure optical fiber," *Opt. Lett.* vol. 26, no. 9, pp. 608-610. May. 2001.

[8] R. Holzwarth, T. Udem, and T. W. Hänsch, et al. "Optical Frequency Synthesizer for Precision Spectroscopy," *Phys. Rev. Lett.* vol. 85, pp. 2264, Sep. 2000.

[9] S. Coen, A. H. L. Chau, R. Leonhardt, J. D. Harvey, J. C. Knight, W. J. Wadsworth, and P. St. J. Russell, "White-light supercontinuum generation with 60-ps pump pulses in a photonic crystal fiber," *Opt. Lett.* vol. 26, no. 17, pp. 1356–1358, Sep. 2001.

[10] G. Genty, M. Surakka, J. Turunen, and A. T. Friberg, "Complete characterization of supercontinuum coherence," *J. Opt. Soc. Am. B*, vol. 28, no. 9, pp. 2301–2309, Sep. 2011.

[11] B. Kuyken, T. Ideguchi, S. Holzner, et al. "An octave-spanning mid-infrared frequency comb generated in a silicon nanophotonic wire waveguide," *Nat. Commun.* vol. 6, Feb. 2015.

[12] F. Li, Q. Li, J. Yuan, et al., "Highly coherent supercontinuum generation with picosecond pulses by using self-similar compression," *Opt. Express*, vol. 22, no. 22, pp. 27339-27354, Nov. 2014.

[13] L. E. Hooper, P. J. Mosley, A. C. Muir, W. J. Wadsworth, and J. C. Knight, "Coherent supercontinuum generation in photonic crystal fiber with all-normal group velocity dispersion," *Opt. Express*, vol. 19, no. 6, pp. 4902-4907, Mar. 2011.

[14] G. Genty, S. Coen, and J. M. Dudley, "Fiber supercontinuum sources," J. *Opt. Soc. Am. B*, vol. 24, no. 8, pp. 1771-1785, Aug. 2007.

[15] J. C. Travers, "Blue extension of optical fibre supercontinuum generation," *J. Opt.* vol. 12, pp. 113001, Nov. 2010.

[16] J. H. Yuan, Z. Kang, F. Li, X. T. Zhang, X. Z. Sang, Q. Wu, B. B. Yan, K. R. Wang, X. Zhou, K. P. Zhong, G. Y. Zhou, C. X. Yu, C. Lu, H. Y. Tam, and P. K. A. Wai, "Mid-Infrared octave-spanning supercontinuum and frequency comb generation in a suspended germanium-membrane ridge waveguide," *J. Lightw. Technol.* vol. 35, no. 14, pp. 2994-3002, Jul. 2017.

[17] C. Conti, M. A. Schmidt, P. S. J. Russell, and F. Biancalana, "Highly noninstantaneous solitons in liquid-core photonic crystal fibers," *Phys. Rev. Lett.* vol. 105, pp. 263902, Dec. 2010.

[18] R. V. J. Raja, A. Husakou, J. Hermann, and K. Porsezian, "Supercontinuum generation in liquid-filled photonic crystal fiber with slow nonlinear response," *J. Opt. Soc. Am. B.* vol. 27, no. 9, pp. 1763–1768, Sep. 2010.

[19] D. Churin, T. N. Nguyen, K. Kieu, R. A. Norwood, and N. Peyghambarian, "Mid-IR supercontinuum generation in an integrated liquid-core optical fiber filled with CS_2," *Opt. Mater. Express*, vol. 3, no. 9, pp. 1358-1364, Sep. 2013.

[20] S. Kedenburg, T. Gissibl, T. Steinle, A. Steinmann, and H. Giessen, "Towards integration of a liquid-filled fiber capillary for supercontinuum generation in the 1.2–2.4 μm range," *Opt. Express*, vol. 23, no. 7, pp. 8281–8289, Apr. 2015.

[21] G. Fanjoux, S. Margueron, J. C. Beugnot, and T. Sylvestre, "Supercontinuum generation by stimulated Raman–Kerr scattering in a liquid-core optical fiber," *J. Opt. Soc. Am. B.* vol. 34, no. 8, pp. 1677–1683, Aug. 2017.

[22] M. Chemnitz, M. Gebhardt, C. Gaida, F. Stutzki, J. K., J. Limpert, A. Tünnermann, and M. A. Schmidt, "Hybrid soliton dynamics in liquid-core fibres," *Nat. Commun.* vol. 8, pp. 42, Jul, 2017.

[23] E. K. Plyler, and C. J. Humphreys, "Infrared absorption spectrum of carbon disulfide," *J. Res. Natl. Bur. Stand*. vol. 39, pp. 59-65, Jul. 1947.

[24] K. Porsezian, R. V. J. Raja, A. Husakou, and J. Hermann, "The contribution of reorientational nonlinearity of CS_2 liquid in supercontinuum generation," Proc. SPIE 8173, 81731D, 2011.

[25] S. Kedenburg, A. Steinmann, R. Hegenbarth, T. Steinle, and H. Giessen, "Nonlinear refractive indices of nonlinear liquids: wavelength dependence and influence of retarded response," *Appl. Phys. B.* vol. 117, pp. 803–816, Dec. 2014.

[26] Y. Sato, R. Morita, and M. Yamashita, "Study on ultrafast dynamic behaviors of different nonlinear refractive index components in CS2 using a femtosecond interferometer," *Jpn. J. Appl. Phys*., Part 1 vol. 36, pp. 2109–2115, Apr. 1997.

[27] R. Zhang, J. Teipel, and H. Giessen, "Theoretical design of a liquid-core photonic crystal fiber for supercontinuum generation," *Opt. Express*, vol. 14, pp. 6800–6812, Jul 2006.

[28] H. E. Kashef, "Optical and electrical properties of materials," *Rev.Sci. Instrum.* vol. 65, pp. 2056–2061, Jan, 1994.

[29] Q. Liu, S. Li, H. Chen, J. Li, and Z. Fan, "High-sensitivity plasmonic temperature sensor based on photonic crystal fiber coated with nanoscale gold film," *Appl. Phys. Exp.* vol. 8, pp. 046701, Apr. 2015.

[30] Boris T. Kuhlmey, Benjamin J. Eggleton, and Darran K. C. Wu, "Fluid-Filled Solid-Core Photonic Bandgap Fibers," *J. Lightwave Technol.* vol. 27, pp. 1617-1630, Jun. 2009.

Zhe Kang received the B.S. degree from Wuhan University of Technology, Wuhan, China, in 2006, the M.S. degree from Dalian Polytechnic University, Dalian, China, in 2012, and the Ph.D. degree from Beijing University of Posts and Telecommunications, Beijing, China, in 2015. Currently he serves as the postdoctoral fellow in The Hong Kong Polytechnic University. His research interests include ultrafast nonlinear optics and nonlinear silicon photonics.

Feng Xu received the Bachelor's degree in optical information science technology from Nanjing University of Posts and Telecommunications (NJUPT), Nanjing, China, in 2016. He is currently working toward the Master's degree in electronic science and technology at Beijing University of Posts and Telecommunications (BUPT), Beijing, China. His research interests include photonic crystal fiber, pulse compression, and supercontinuum generation.

Jinhui Yuan received the B.S. and M.S. degrees from Yanshan University, Qinhuangdao, China, in 2005 and 2008, respectively. In 2011, he received the Ph.D. degree from Beijing University of Posts and Telecommunications (BUPT), Beijing, China. Now he is with the BUPT as an associate professor. He is also a Hong Kong Scholar at the Photonics Research Centre, Department of Electronic and Information Engineering, The Hong Kong Polytechnic University. His current research interests include photonic crystal fibers, silicon waveguide, and optical fiber devices. He is the Senior Members of IEEE and OSA. He has published over 150 papers in the academic journals and conferences.

Feng Li received the B.S. and Ph.D. degrees from University of Science and Technology of China, Hefei, China, in 2001 and 2006, respectively. After that, he joined the Hong Kong Polytechnic University as a postdoctoral fellow. Currently he is a research fellow the Hong Kong Polytechnic University. His research interests include fiber lasers, especially multiwavelength lasers and mode locked lasers, nonlinear fiber optics, supercontinuum generation, and nonlinear dynamics in optical devices and optical systems. He is the Senior Member of OSA.

Binbin Yan received the B.S. and M.S. degrees from Beijing University of Posts and Telecommunications (BUPT), Beijing, China, in 2003 and 2005, respectively. In 2009, she received the Ph.D. degree from BUPT.

Now she is with the BUPT as a lecturer. Her research interests include photonic devices and fiber optic sensing.

Xian Zhou received the Ph.D. degree in electromagnetic field and microwave technology from Beijing University of Posts and Telecommunications (BUPT), Beijing, China, in 2011. She is currently an Associate Professor at the Department of computer and communication engineering, University of Science and Technology Beijing (USTB). She is also a Hong Kong Scholar at the Photonics Research Centre, Department of Electronic and Information Engineering, The Hong Kong Polytechnic University. Her research interests are focused on high-speed optical communications, short reach communications and digital signal processing.

Qiang Wu received the B.S. and Ph.D. degrees from Beijing Normal University and Beijing University of Posts and Telecommunications, Beijing, China, in 1996 and 2004, respectively. From 2004 to 2006, he worked as a senior research associate in City University of Hong Kong. From 2006 to 2008, he took up a research associate post in Heriot-Watt University, United Kingdom. From 2008 to 2014, he worked as a Stokes lecturer at Photonics Research Centre, Dublin Institute of Technology, Ireland. Currently he is an associate professor at Northumbria University, United Kingdom. His research interests include photonics devices and fiber optic sensing.

Kuiru Wang received the B.S. M.S. degrees from Beijing University of Posts and Telecommunications (BUPT), Beijing, China, in 1984 and 1990, respectively. In 2009, she received the Ph.D. degree from BUPT. Now she is with the BUPT as a professor. Her current research interests include optical fiber communication and photonic devices.

Xinzhu Sang received the B.S. degree from Tianjin University, Tianjin, China and the M.S. degree from Beijing Institute of Machinery, Beijing, China, in 1999 and 2002, respectively, and the Ph.D. degree from Beijing University of Posts and Telecommunications (BUPT), Beijing, China, in 2005. Now he is with the BUPT as a professor. From December 2003 to March 2005, he was with Optoelectronics Research Centre, Department of Electronic Engineering, City University of Hong Kong as a research assistant. From July 2007 to July 2008, he worked in University of California at Irvine as a postdoctoral research scholar. His current research interests include novel photonic devices, optical communication and optical interconnect. Prof. Sang is a senior Member of Chinese Institute of Communication, a committee of Holography and Optical information Processing, Chinese Optical Society, and a member of OSA.

Keping Long (SM'06) received the M.S. and Ph.D. degrees from the University of Electronic Science and Technology of China, Chengdu, China, in 1995 and 1998, respectively. From September 1998 to August 2000, he was a Postdoctoral Research Fellow with the National Laboratory of Switching Technology and Telecommunication Networks, Beijing University of Posts and Telecommunications (BUPT), Beijing, China. From September 2000 to June 2001, he was an Associate Professor with BUPT. From July 2001 to November 2002, he was a Research Fellow with the ARC Special Research Centre for Ultra Broadband Information Networks, University of Melbourne, Melbourne, Australia. He is currently a Professor and Dean with the School of Computer and Communication Engineering, University of Science and Technology Beijing. He has authored more than 200 papers and has delivered 20 keynote speeches. He is a Member of the Editorial Committee of Sciences in China Series F and China Communications. His research interests are optical internet technology, new-generation network technology, wireless information networks, value-added service, and secure technology of networks. Dr. Long has been a Technical Program Committee (TPC) and International Steering Committee member for COIN2003/04/05/06/07/08/09/10, IEEE IWCN2010, ICON04/06, and APOC2004/06/08; a Co-chair of the organization membership for the 2006 International Wireless Communications and Mobile Computing Conference; the TPC chair of COIN2005/2008; and a TPC Cochair of COIN2008/2010. He has been invited to talk at both international and local conferences. He received the National Science Fund for Distinguished Young Scholars of China in 2007 and was selected as the Chang Jiang Scholars Program Professor of China in 2008.

Chongxiu Yu graduated from the Beijing University of Posts and Telecommunications (BUPT), Beijing, China, in 1969. Now he is with the BUPT as a professor. She is engaged in university education and research work and has been the Principal Investigator of many projects supported by China 863 plan, the National Natural Science Foundation and the National Ministry of Science Technology, and so on. Up to now she has published more than 300 papers. Her Research interests are the optical fiber communication, photonic switching, and optoelectronics technology and its applications. Prof. Yu is the Members of Chinese Institute of Communication, Committee of Fiber Optics and Integral Optics, and Chinese Optical Society.